JACS
JOURNAL OF THE AMERICAN CHEMICAL SOCIETY
Article
pubs.acs.org/JACS

Mechanism for the Enhanced Excited-State Lewis Acidity of Methyl Viologen

Edward G. Hohenstein*[,†,‡]

[†]Department of Chemistry and Biochemistry, The City College of New York, New York, New York 10031, United States
[‡]Ph.D. Program in Chemistry, The Graduate Center of the City University of New York, New York, New York 10016, United States

Supporting Information

ABSTRACT: Aqueous solutions of methyl viologen (MV^{2+}) exhibit anomalous fluorescence behavior. Although it has long fluorescence lifetimes in polar solvents such as acetonitrile, MV^{2+} has a short fluorescence lifetime in water. Recent experiments by Kohler and coworkers (Henrich et al. *J. Phys. Chem. B* **2015**, *119*, 2737−2748) have implicated an excited-state acid/base reaction as the source of the nonradiative decay pathway. While many chemical species exhibit enhanced Brønsted acidity in their excited state, MV^{2+} is the first example of a species with enhanced Lewis acidity. Using a complete active space configuration interaction (CASCI) approach, excited-state molecular dynamics simulations of aqueous MV^{2+} are performed in order to test the hypothesis that MV^{2+} acts as a Lewis photoacid and to elucidate a mechanism for this behavior. These simulations show that the Lewis acidity of MV^{2+} is indeed enhanced by photoexcitation. On its S_1 excited state, MV^{2+} reacts with water to generate a hydronium ion approximately 1.5 ps after excitation. After the hydronium ion is produced, the corresponding hydroxide ion adds to MV^{2+} to form a covalently bound photoproduct and, subsequently, evolves toward a conical intersection.

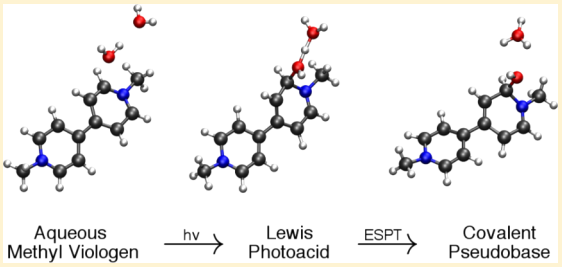

INTRODUCTION

It has long been understood that molecules containing labile protons are stronger acids in their electronic excited states than in their ground state. These Brønsted photoacids have been the subject of extensive investigation over the last 65 years. As a result, many compounds that exhibit this behavior are known and the mechanism of excited-state proton transfer is well-understood in these systems. This effect was initially characterized by Förster and Weller in the context of naphthol derivatives.[1−4] As experimental techniques advanced, studies of pyranine by Pines, Huppert, and collaborators provided a more detailed mechanistic understanding of photoacidity.[5−8] Since then, pyranine has been used in a variety of studies of proton transfer dynamics.[9−13] Similarly, naphthols also form an important class of photoacids.[3,4,14] Naphthols are particularly interesting because many substituted variants exist and have a wide range of acidities as well as proton transfer rate constants.[15−27] Derivatives of hydroxyquinoline act as particularly strong photoacids and have been studied extensively by several groups.[28−32] Over the past few years, Huppert and coworkers have placed an emphasis on developing quinone cyanine photoacids that can dissociate within 100 fs of excitation.[33−35] These quinone cyanine photoacids likely represent the upper limit for the rate of proton transfer to solvent.[36]

Since photoacids are capable of generating protons on an extremely short time scale, this property has been exploited to study dynamical processes in solution. Perhaps the most common use for photoacids is as a probe of acid dissociation dynamics.[14,36−41] Other processes such as acid-catalyzed reactions, protein folding, or drug delivery can be initiated by using photoacids to create rapid pH changes in a solution.[42,43] The synthesis of new photoacids that are well-suited to this purpose is still an active area of research.[44−46] In this case, the goal is to design a molecule that not only can quickly release a proton but also has a back reaction that occurs very slowly. The development of new photoacids continues to increase the types of environments and time scales where these molecules can be used. In addition, excited-state proton transfer reactions are also important in biological systems. For example, the chromophore of the green fluorescent protein and some of its mutants exhibits photoacidic behavior;[47−49] also, excited-state proton transfer has been implicated in the fluorescence quenching of photoexcited tryptophan residues.[50,51]

Recently, it was proposed that the Lewis acidity of certain molecules can also be enhanced by photoexcitation.[52] That is, a molecule without a labile proton could initiate a proton transfer event in the surrounding solvent. Spectroscopic evidence suggests that the molecule, methyl viologen, 1,1′-dimethyl-4,4′-bipyridinium or, commonly, paraquat (MV^{2+}), acts as a Lewis photoacid. Although the exact mechanism for this enhanced Lewis acidity remains unknown, it appears to be closely linked to a novel pathway for nonradiative decay. Understanding this mechanism promises to lead to the

Received: August 4, 2015
Published: January 4, 2016

DOI: 10.1021/jacs.5b08177
J. Am. Chem. Soc. 2016, 138, 1868−1876

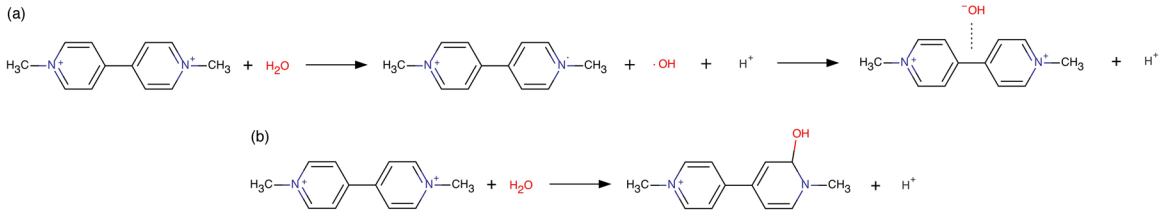

Figure 1. Two proposed reaction mechanisms for the photophysics of MV^{2+}.[52] (a) After photoexcitation, MV^{2+} oxidizes water to generate hydroxyl radical and a proton. Subsequently, a back electron transfer occurs that generates a long-lived complex between MV^{2+} and a hydroxide ion. (b) Water adds covalently to MV^{2+}, forming a pseudobase, $MVOH^+$, and releasing a proton.

identification of molecules that share this behavior and other contexts where this decay pathway might be relevant.

MV^{2+} has many chemical applications as a strong electron acceptor ranging from its use as a herbicide[53] to its use in the photochemical conversion of solar energy.[54−59] The reduced form of MV^{2+} has a distinct spectroscopic signature, which gives the molecule its name and allows it to be used as a redox indicator.[60] In 2001, Kohler and co-workers examined the photoreduction of MV^{2+} in a variety of solvents.[61] In solvents with relatively low ionization potentials, the photoreduction of MV^{2+} and concomitant quenching of fluorescence was observed. In methanol, for example, MV^{2+} has an excited-state lifetime of less than 180 fs. In solvents with higher ionization potentials, such as acetonitrile, no photoreduction is observed, MV^{2+} fluoresces with a high quantum yield, and it has an excited-state lifetime of about 1 ns. Following this trend, it would be expected to see a long lifetime and high fluorescence yield in water, since it has an even higher ionization potential than acetonitrile. However, neither photoreduction nor a long fluorescence lifetime is observed. Instead, aqueous solutions of MV^{2+} exhibit quenched fluorescence and a short lifetime of only 3.1 ps. Regarding this result, Kohler and co-workers state[61]

> *"Perhaps a single water molecule can control access to the conical intersection that is responsible for isomerization. Alternatively, the water molecule could itself be a reactant in an as yet uncharacterized photoreaction of MV^{2+}*. In preliminary experiments, we have detected a residual transient absorption near 300 nm in bulk water that may be assignable to an MV^{2+} isomer or a novel photoproduct."*

The behavior of MV^{2+} in water was recently revisited by Kohler and co-workers under the hypothesis that this uncharacterized photoreaction was a result of enhanced Lewis acidity in photoexcited MV^{2+}.[52] This hypothesis was supported by showing that the changes in the steady-state absorption spectrum of MV^{2+} with increasing pH are nearly identical to the transient absorption spectrum of aqueous MV^{2+} 1 ns after excitation. For the first time, evidence has been presented that supports the existence of a molecule with enhanced Lewis acidity in its excited state.

Several different mechanisms for the Lewis acidity of MV^{2+} were considered by Kohler and co-workers.[52] One possibility is that a hydroxide ion adds to MV^{2+}, forming a covalent adduct (or pseudobase) (Figure 1b).

$$MV^{2+} + H_2O \rightarrow MVOH^+ + H^+ \quad (1)$$

This pseudobase has been proposed to be the conjugate base of MV^{2+}; however, it has never been isolated.[62,63] Kohler and co-workers rule out this mechanism on the basis of thermodynamic and kinetic arguments: MV^{2+} is found to be a "vanishingly weak" Lewis acid in its ground electronic state, which means that the Lewis acidity must be photoenhanced by many orders of magnitude, and the authors found it unlikely that covalent addition of water to MV^{2+} could occur within the fluorescence lifetime of 3.1 ps.[52] Instead, it was proposed that photoexcited MV^{2+} oxidizes water (Figure 1a).

$$MV^{2+} + H_2O \rightarrow MV^{\bullet+} + OH^{\bullet} + H^+ \quad (2)$$

Subsequently, an ultrafast back electron transfer occurs that generates a long-lived noncovalent complex between MV^{2+} and the hydroxide ion.

$$MV^{\bullet+} + OH^{\bullet} \rightarrow MV^{2+} \cdots OH^- \quad (3)$$

However, the spectroscopic signature of $MV^{\bullet+}$ or the hydroxyl radical, $OH^{\bullet}$, was not detected. This is in contrast to the transient absorption spectrum of photoexcited MV^{2+} in methanol where the contributions from $MV^{\bullet+}$ are quite pronounced.[61] Due to a lack of direct evidence for either of the proposed mechanisms, the exact nature of the reaction remains a matter of speculation.

In the present work, the photochemistry of aqueous MV^{2+} will be directly simulated using excited-state molecular dynamics. The purpose is 2-fold: to either corroborate or refute the enhanced Lewis acidity of MV^{2+} and to discover the mechanism for this enhanced Lewis acidity if it indeed exists. Excited-state molecular dynamics simulations have provided insight into a wide variety of photochemical processes; however, these simulations are largely limited to small molecules in the gas phase and systems where the photochemistry does not involve reactions with the environment.[64−67] Simulations of excited-state proton transfer reactions are uniquely challenging because the solvent is an active participant in the reaction and cannot be approximated as a continuum or with a molecular mechanics force field; therefore, hundreds of atoms must be included in the excited-state computations to avoid biasing the simulation to a particular outcome. In addition, these solvent molecules must be treated on the same footing as the chromophore to preserve indistinguishability among the protons. In the present context, this means that a single excited-state computation must include at least 300 atoms. These constraints have limited theoretical investigations to ground-state analogues of excited-state proton transfer.[68−71] Recent advances in computer hardware and electronic structure algorithms make it possible to perform molecular dynamics simulations of excited-state proton transfer reactions.[72,73]

METHODS

All computations are performed using the graphical processing unit (GPU) accelerated quantum chemistry package, TeraChem.[74−76] The bulk of the computations in this work use the fractionally occupied molecular orbital complete active space configuration interaction (FOMO-CASCI) method.[73,77−80] In this method,

DOI: 10.1021/jacs.5b08177
J. Am. Chem. Soc. 2016, 138, 1868−1876

molecular orbitals are obtained from the fractional occupation number Hartree−Fock (FON-HF) method, where a temperature is introduced and the average energy of an ensemble of HF wave functions is minimized.[81,82] A temperature parameter, β, of 0.35 au is used in this work.[73] Once the molecular orbitals are generated, a CASCI wave function is constructed using a CAS(6/4) active space. The molecular orbitals included in the active space are shown in Figure 2. This wave

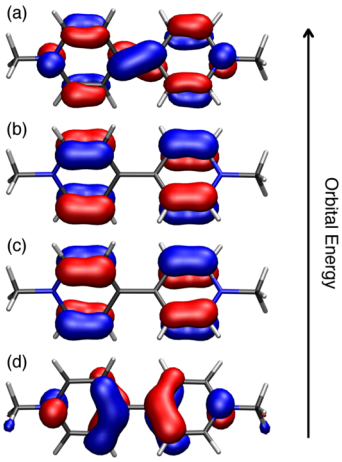

Figure 2. Molecular orbitals of MV^{2+} included in the FOMO-CAS(6/4)-CI active space shown in order of increasing energy. These are canonical FON-HF/6-31G* orbitals evaluated at the ground-state equilibrium geometry of MV^{2+}. The orbital shown in (a) is the lowest-lying π^* orbital of MV^{2+}. The orbitals shown in (b) and (c) are the highest-lying π orbitals of MV^{2+} and are nearly degenerate. The orbital shown in (d) is another high-lying π orbital that is included in the active space. The S_1 excited state is characterized by a single excitation from one of the two nearly degenerate orbitals, (b) and (c), to the π^* orbital, (a). The orbital shown in (d) is doubly occupied on the S_1 state and does not directly contribute to the reaction between MV^{2+} and water; however, it is included in the active space to maintain continuity of the potential energy surface throughout the region of interest. These orbitals are obtained from gas-phase computations.

function contains all determinants generated from combinations of six electrons in four orbitals. The fractionally occupied FON-HF orbitals are also restricted to a similar (6/4) space. The performance of FOMO-CASCI compares favorably to both complete active space self-consistent field (CASSCF)[83] and multistate second-order perturbation theory (MS-CASPT2)[84,85] for the excited states of MV^{2+}; details can be found in the Supporting Information.

In order to study the photochemistry of aqueous MV^{2+}, a sphere of water molecules with a radius of 25 Å is constructed (Figure 3). A QM/MM partitioning[86] is used where at least the 100 water molecules nearest to MV^{2+} are included in the FOMO-CASCI computations. The remaining water molecules are treated with the three-site transferable intermolecular potential (TIP3P)[87] model. The effect of the MM water molecules is included in the FOMO-CASCI computations through the atomic point charges in the TIP3P model. A soft, harmonic spherical restraining potential is applied to prevent evaporation during the dynamics simulations and to constrain the density inside the sphere to be 1 g mL^{-1}. The harmonic restraint uses a force constant of 10 kcal mol^{-1} $Å^{-2}$. Finally, Grimme's D3 empirical dispersion correction[88] is applied to the atoms in the QM region to model the effect of the long-range dynamic electron correlation that is missing in the FOMO-CASCI method when a small active space is used. The parameters of the D3 dispersion correction are those optimized for HF.

Classical molecular dynamics simulations are performed on the first singlet excited state of MV^{2+}; energies and forces are evaluated on-the-fly with the FOMO-CAS(6/4)-CI method. Although it is the transition to S_3 that is optically accessible, rapid decay from S_3 to S_1

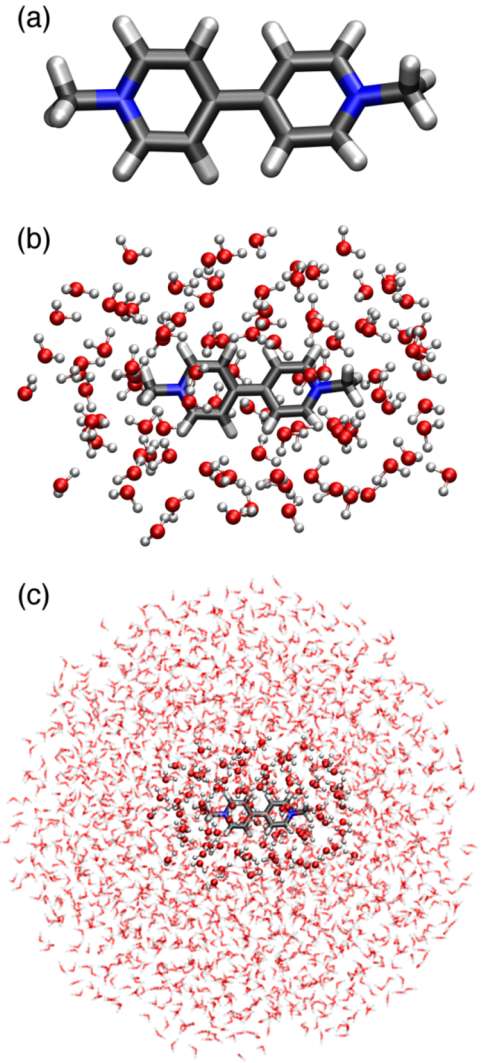

Figure 3. Representative geometries of aqueous MV^{2+} are shown: (a) MV^{2+}, (b) MV^{2+} and 100 water molecules, this is the QM region of the QM/MM simulations, and (c) the full system included in the QM/MM simulations.

is expected from Kasha's rule.[89] Indeed, S_3/S_2 and S_2/S_1 intersections are located near the Franck−Condon point both geometrically and energetically (details are provided in the Supporting Information). Furthermore, only the signature of the S_1 state is observed in transient absorption experiments.[61] The purpose of the present work is to identify a mechanism for Lewis photoacidity, so it is sufficient to consider the adiabatic dynamics of the S_1 state. To obtain independent initial positions and velocities for the excited-state molecular dynamics simulations, a 150 ps NVT molecular dynamics simulation was performed for MV^{2+} in a periodic octahedral box containing 20 196 water molecules. Water molecules are treated with TIP3P and MV^{2+} with the general AMBER force field (GAFF). Subsequently, a 2.5 ns NVT molecular dynamics simulation was performed for this system; every 100 ps the positions and velocities were used to initialize NVT ground-state QM/MM dynamics simulations of methyl viologen. The QM/MM dynamics simulations were performed for 10 ps with MV^{2+} treated at the HF/6-31G level of theory and all water molecules are treated with TIP3P. The excited-state molecular dynamics simulations are initialized from the final positions and velocities of the ground-state QM/MM simulations. All NVT simulations are held at 300 K with a Langevin thermostat (with a collision frequency of 1 ps^{-1}).

Following the generation of the initial conditions described above, NVE simulations of the first excited state of MV^{2+} are performed using FOMO-CAS(6/4)-CI until the energy gap between S_1 and S_0 falls

DOI: 10.1021/jacs.5b08177
J. Am. Chem. Soc. 2016, 138, 1868−1876

below 0.1 eV or after a proton transfer reaction occurs. Since the excited-state simulations are adiabatic in nature, their interpretation becomes ambiguous after a region of intersection between adiabatic states is encountered. The results that will be subsequently discussed are obtained from 25 independent trajectories. Using a recently developed algorithm for FOMO-CASCI energies and gradients, 1 ps of excited-state dynamics (2000 energy and gradient evaluations with 100 water molecules and a 6-31G basis set) takes approximately 3 to 3.5 days on a single workstation.[90] As a check, five of the simulations were performed with modified parameters: two included 150 water molecules in the QM region, one included 200 water molecules in the QM region, and the other two used a larger 6-31G* basis set. The behavior of MV^{2+} in all trajectories was qualitatively similar. This indicates that the number of water molecules in the QM region and the smaller basis set do not significantly change the predicted photochemistry of MV^{2+}.

RESULTS

In 24 of the 25 molecular dynamics trajectories, MV^{2+} is observed to act as a Lewis acid. This is in agreement with Kohler and co-workers' interpretation of their spectroscopic result[52] and provides independent corroboration that the Lewis acidity of MV^{2+} is enhanced by photoexcitation. In these simulations, hydronium ions are generated at an average of 1.5 ± 1.2 ps after photoexcitation. From these simulations, a mechanism for the enhanced Lewis acidity of MV^{2+} may be identified. The important steps that follow excitation can be found in Figure 4. The first step of the reaction is the formation

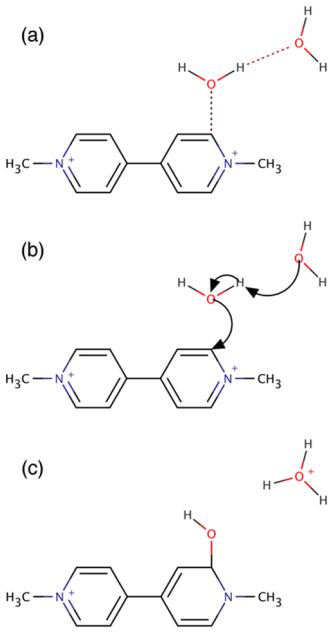

Figure 4. Predicted mechanism for the excited-state Lewis acidity of MV^{2+}. (a) The reaction is preceded by the formation of a complex between MV^{2+} and a water molecule. (b) In a concerted step, intermolecular proton transfer to water and hydroxide addition to MV^{2+} occurs. (c) Products of the reaction.

of an intermediate complex consisting of a water molecule and MV^{2+} (Figure 4a). This is the rate-limiting step because it involves the rearrangement of the hydrogen-bonding network in the surrounding water molecules. Once this complex has been formed, the acid/base reaction occurs (Figure 4b). The complexed water molecule transfers a proton to a neighboring water molecule, and the newly formed hydroxide ion adds to MV^{2+}. The products of the reaction (Figure 4c) are a hydronium ion and a covalently bonded photoproduct. It is the unexpected mechanism of covalent addition (eq 1) that is observed in these simulations. This disagrees with the speculations of Kohler and co-workers that covalent addition of water to MV^{2+} could not occur on a time scale of several picoseconds. This suggests that the excited-state behavior of MV^{2+} is quite different from the ground-state behavior of other Lewis acids.

Immediately following the acid/base reaction, the aqueous MV^{2+} system is in a region of the S_1 potential energy surface that is above S_0 by less than 1 eV. After the reaction occurs, the system evolves toward a conical intersection; the vicinity of a conical intersection (here, a S_1/S_0 gap of less than 0.1 eV is used as an indication that a conical intersection is nearby) is typically reached within approximately 100 fs. As was proposed by Kohler and co-workers,[61] it is the reaction with water that provides access to a conical intersection and mediates nonradiative decay. For example, Figure 5 shows the S_1/S_0 gap (in black) as a function of time for a representative molecular dynamics trajectory (similar figures can be found in the Supporting Information for the other molecular dynamics trajectories). In this case, the acid/base reaction occurs at roughly 250 fs, and the S_1/S_0 gap becomes very small approximately 50 fs later. The present dynamical simulations are restricted to a single electronic state (S_1) because we do not include surface "hopping"[91] or "spawning".[92,93] Therefore, the dynamics past the time when a trajectory approaches a conical intersection cannot be followed. This prevents the prediction of an excited-state lifetime for MV^{2+} on S_1, but 1.5 ps can be estimated as a lower bound of the excited-state lifetime. However, the S_1 state of aqueous MV^{2+} is well-separated (±1 eV) from the other electronic states during the acid/base reaction, so the present approach dynamics is sufficient to study the reaction mechanism on S_1. In one of the 10 trajectories, no acid/base reaction is observed. In this case, MV^{2+} approached a conical intersection via torsion along the central carbon−carbon bond (the time evolution of this torsional angle can be found in the Supporting Information for each molecular dynamics trajectory). The dominant pathway for nonradiative decay is clearly the Lewis acid/base reaction; however, the present simulation does not include the nonadiabatic effects necessary to provide a quantitative estimate of the branching ratio.

The rates of both the formation of the intermediate complex as well as the generation of the hydronium ion are limited by solvent motion. In Figure 5, certain key interatomic distances are shown as a function of time for one of the molecular dynamics trajectories. For clarity, a reaction that occurred quickly (about 250 fs) was chosen. The carbon−oxygen distance that is shown will become a carbon−oxygen bond in the photoproduct. When this distance reaches roughly 1.6 Å, it can be said that the intermediate complex between the water molecule and MV^{2+} has been formed. The rate of this step is controlled by the time it takes the hydrogen-bonding network to rearrange and the water molecule to complex with MV^{2+}. The complex forms via the interaction of the water molecule's lone pairs with the electron-deficient carbon atom in the 2-position of MV^{2+}. This complex exists until a second water molecule moves into position to accept the proton. The distance between this second water molecule and the reactive water is shown in red in Figure 5. Notice that the intermediate complex exists until the acceptor water molecule approaches within approximately 2.3 Å of the donor; at this point, the

DOI: 10.1021/jacs.5b08177
J. Am. Chem. Soc. 2016, 138, 1868−1876

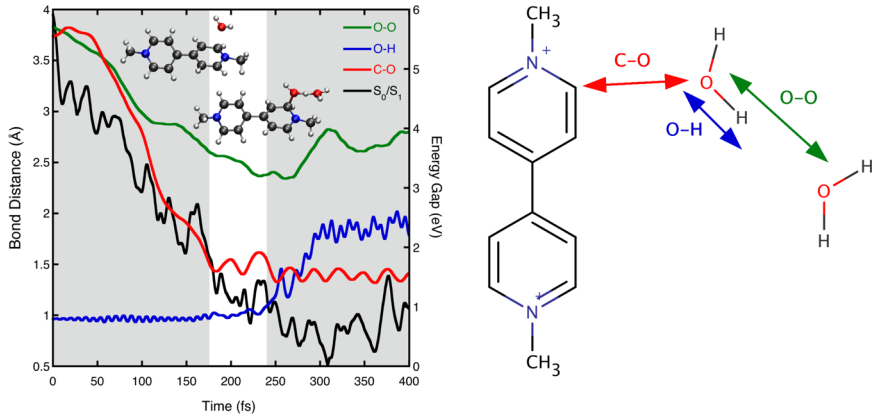

Figure 5. A few bond distances relevant to the Lewis acidity of MV^{2+} as a function of time for the first 400 fs of a representative molecular dynamics trajectory. The carbon−oxygen distance for the bond formed in the product state is shown in red. The oxygen−oxygen distance corresponding to the proton donor and acceptor water molecules is shown in green. The hydrogen−oxygen distance corresponding to the reactive water molecule is shown in blue. Finally, the gap between the lowest and first excited singlet states is shown in black. The gray shading on the left (0−175 fs) represents the system in what is best described as its reactant state. The white region represents an intermediate state (175−250 fs). The gray shading on the right represents the product state (250−400 fs). Similar figures can found in the Supporting Information for the other molecular dynamics trajectories.

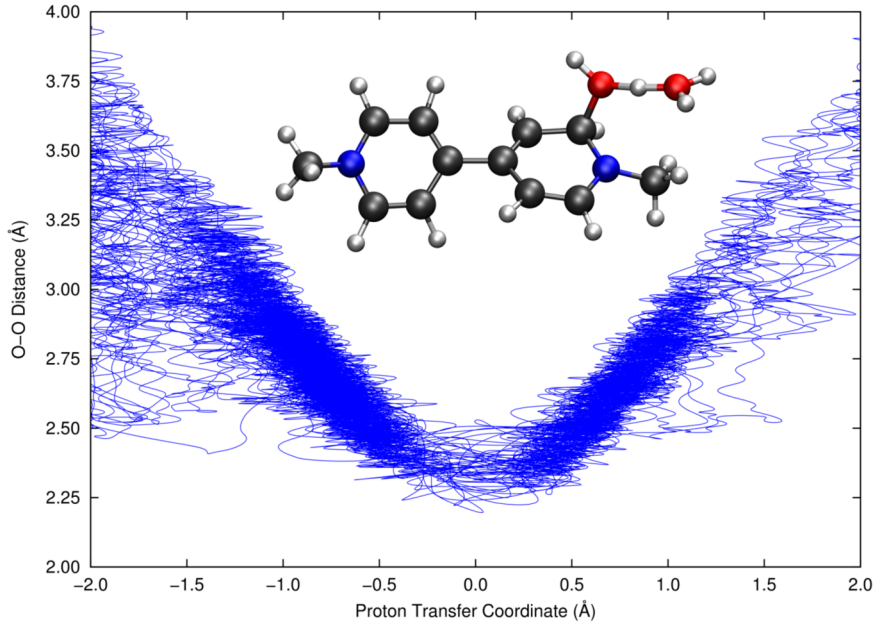

Figure 6. Time evolution of the oxygen−oxygen distance and proton transfer coordinate corresponding to each of the 24 reactive excited-state molecular dynamics trajectories (shown in Å). The oxygen−oxygen distance is the distance between proton donor (O_D) and acceptor (O_A) atoms. The proton transfer coordinate is defined as $R_{O_DH} - R_{O_AH}$. The proton transfer coordinate is zero during the reaction when the proton is equidistant from the donor and acceptor. On average, time flows from the top left to the top right.

proton transfer can occur (this oxygen−oxygen distance is similar to that found in the Zundel cation, $H_5O_2^+$). The relationship between proton transfer and the distance between donor and acceptor molecules is shown in Figure 6. The acceptor water molecule gates the proton transfer reaction; no proton transfer events are observed when the acceptor oxygen is more than 2.5 Å away from the donor. After proton transfer, the carbon−oxygen distance never again exceeds 1.5 Å, indicating the formation of a covalent bond. This same general behavior is observed in the other reactive trajectories: the rate is limited by the formation of the intermediate complex between water and MV^{2+} and the proton transfer step occurs shortly thereafter (usually within 100 fs) once an acceptor water is in position. This is further illustrated in Figure 7. Here, the reactive water molecule can be seen approaching MV^{2+} and eventually forming a complex (characterized by a carbon−oxygen distance of less than 1.6 Å); subsequently, the proton transfer occurs. Notice that this acid/base reaction is best described with a sequential mechanism. A concerted reaction is observed only in one of 24 trajectories where the formation of the complex between MV^{2+} and water does not form before proton transfer occurs.

In all simulations where a reaction was observed, the hydroxide adds to the 2-position of MV^{2+} (Figure 4). To rationalize this result, the redistribution of charge upon electronic transition in aqueous MV^{2+} is considered. Since, in solution, the geometry is no longer symmetric, the near degeneracy between the two highest-lying π orbitals is lifted

DOI: 10.1021/jacs.5b08177
J. Am. Chem. Soc. 2016, 138, 1868−1876

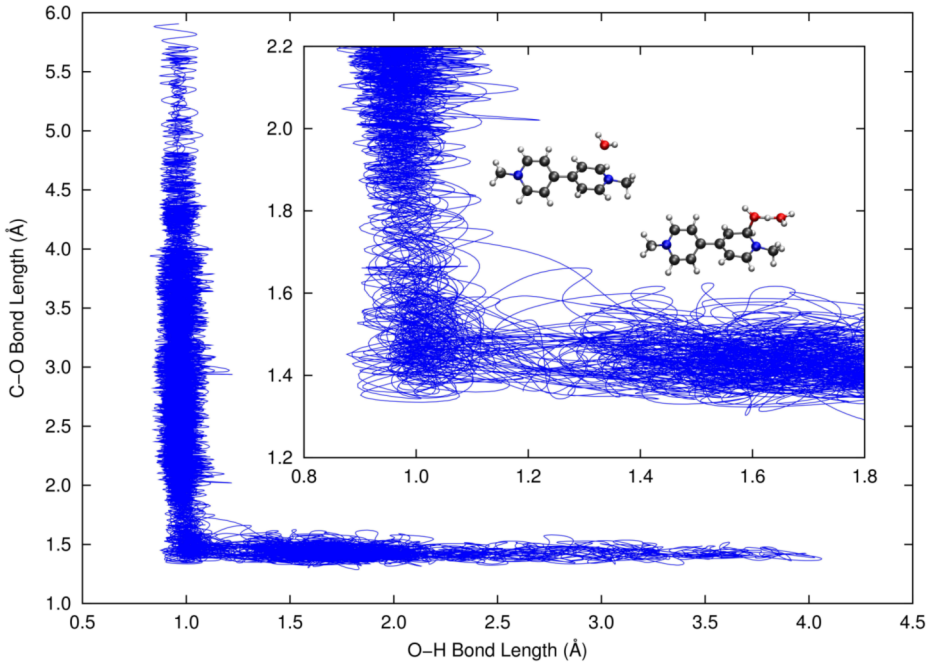

Figure 7. Time evolution of the carbon–oxygen distance for the bond formed in the product state and the hydrogen–oxygen distance corresponding to the proton transfer reaction in each of the 24 reactive excited-state molecular dynamics trajectories (shown in Å). In the inset, the region where the proton transfer reaction occurs is shown in detail. On average, time flows from the top left to the bottom right.

(i.e., Figure 2b,c). These orbitals localize on one of the aromatic rings, and, as a result, the near degeneracy between the S_1 and S_2 states is lifted. The localization of the π orbitals breaks the symmetry of MV^{2+} in its excited state and directs the reaction toward one of the two rings. The charge redistribution is quantified as the change in atomic charge between the ground and excited state (Figure 8). Qualitatively, the changes that result from transitions to S_1 and S_2 are very similar (Figure 8a,b, respectively). In these states, the aromatic carbon atoms in the 2-position have an increased positive charge (by approximately 0.2 au). By comparison, the charge redistribution associated with a transition to S_3 is minor. There is also an enhancement of positive charge at one the 3-positions in the S_1 and S_2 states; however, the total charge at this position is negative (Figure 9). Reactions are observed only at the 2-position, where the overall total charge is positive. As MV^{2+} relaxes on the S_1 state after photoexcitation, the positive variation in charge at the 2-position is further enhanced (Figure 9). This suggests that the rearrangement of charge that occurs upon excitation to S_1 is maintained throughout the excited-state dynamics and increases the reactivity of MV^{2+} at the 2-position.

It remains unclear whether the photoproduct observed in experiment is the covalently bound $MVOH^+$ predicted by the present simulations, the $MV^{2+}\cdots OH^-$ complex proposed by Kohler and co-workers,[52] or the result of a different process entirely. In the aqueous MV^{2+} system, the predicted photoproduct contains the only carbon–oxygen bond. Therefore, time-resolved infrared spectroscopy would be an obvious choice to provide experimental verification of these predictions. Transient absorption in the vicinity of 1100 cm^{-1} by aqueous MV^{2+} would be an indication of the formation of a covalently bonded pseudobase. At this time, the fate of the photoproduct, $MVOH^+$, has not been determined, definitively, via simulation. The reaction between MV^{2+} and water provides a nonradiative decay pathway; nonadiabatic dynamics simulations will be needed in order to properly capture the electronic transition

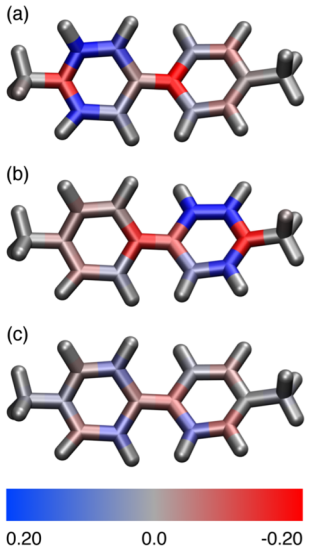

Figure 8. Change in the atomic (Mulliken) charges in atomic units of aqueous MV^{2+} between the ground state and (a) S_1, (b) S_2, and (c) S_3 excited states at the FOMO-CAS(6/4)-CI/6-31G* level of theory. An increase in the atomic charge (depletion of electron density) is represented in blue. A decrease in the atomic charge is represented in red (an increase in the electron density). No change in the atomic charge is represented in gray. The molecular geometry is the initial state of an excited-state molecular dynamics trajectory; this geometry is in the potential well associated with the S_0 minimum. All water molecules are treated with TIP3P.

back to the ground state. From examination of the adiabatic simulations, it appears that these nonadiabatic transitions will be possible sometime after the noncovalent complex of water and MV^{2+} forms (or by twisting about the central carbon–carbon bond). If the decay back to S_0 occurs before the proton transfer reaction can occur, then the carbon–oxygen bond

DOI: 10.1021/jacs.5b08177
J. Am. Chem. Soc. 2016, 138, 1868–1876

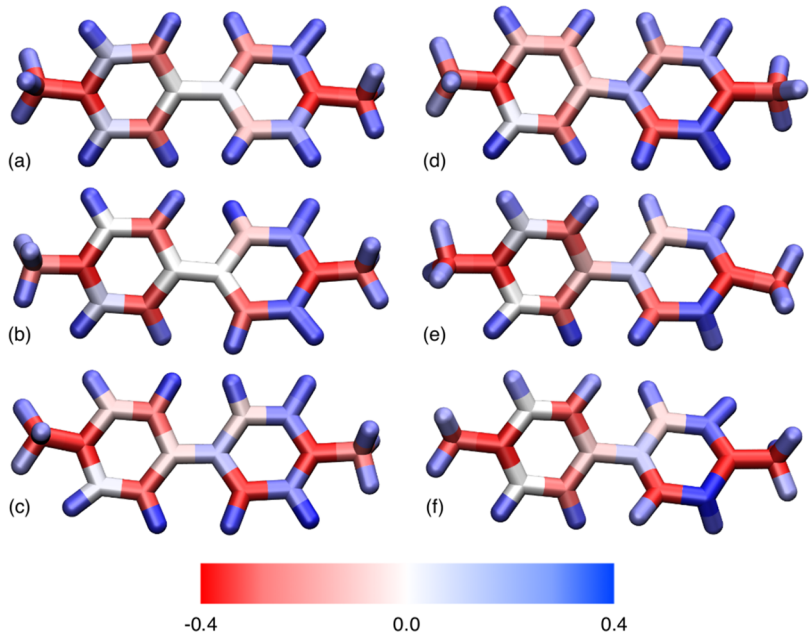

Figure 9. Total atomic (Mulliken) charge in atomic units of aqueous MV^{2+} at the FOMO-CAS(6/4)-CI/6-31G* level of theory for six snapshots from the molecular dynamics trajectory shown in Figure 5. Snapshots are taken after (a) 0, (b) 50, (c) 100, (d) 150, (e) 200, and (f) 250 fs. Negative atomic charges are represented by red coloring; positive atomic charges are represented by blue. The same QM/MM partitioning used in the excited-state dynamics simulation is used here, namely, 100 water molecules are included in the QM region and the remainder are treated with TIP3P. For clarity, only MV^{2+} is shown.

between the water molecule and MV^{2+} will rapidly dissociate (within tens of femtoseconds). If the proton transfer reaction precedes decay back to S_0, then the fate of $MVOH^+$ will depend on how far the proton has diffused. Preliminary ground-state molecular dynamics simulations of $MVOH^+$ in neat water suggest that the hydroxide will remain covalently bonded for more than 1 ps and not dissociate upon decay back to S_0. However, when a hydronium ion is present in the first solvation shell, the reverse reaction occurs rapidly on the ground state (within hundreds of femtoseconds). These results are consistent with the shorter experimental lifetimes of the photoproduct in acidic solutions.

CONCLUSIONS

Recent experiments have proposed that MV^{2+} exhibits enhanced Lewis acidity in its excited state. In the present work, ab initio excited-state molecular dynamics simulations of aqueous MV^{2+} have been performed that confirm this proposal. In addition, the mechanism for Lewis photoacidity has been determined on the basis of these simulations. Charge redistribution on the S_1 state makes MV^{2+} more susceptible to attack by a water molecule in the 2-position. This reaction proceeds first by the formation of a complex of excited MV^{2+} and the reacting water molecule. Then, in a concerted step, this water molecule releases a proton and the newly generated hydroxide ion adds covalently to MV^{2+}. These simulations provide a surprising answer to the question of how MV^{2+} acts as a photoacid. In light of these results, new experiments should be performed to look for the spectroscopic signature of this covalently bonded photoproduct.

This new understanding of how a molecule can act as a Lewis photoacid makes it possible to begin searching for other species that exhibit the same behavior. Aromatic molecules with low-lying charge-transfer excited states, no labile protons, and short fluorescence lifetimes in aqueous solutions are possible candidates for enhanced excited-state Lewis acidity. Derivatives of 4,4′-bipyridine provide an obvious starting point for such a search; 4,4′-bipyridinium is not fluorescent in water and is likely to be another example of a Lewis photoacid. Interestingly, aqueous solutions of related compounds such as hexamethyl viologen (1,1′,2,2′,6,6′-hexamethyl-4,4′-bipyridinium)[94] or diquat (1,1′-ethylene-2,2′-bipyridylium)[95] do exhibit fluorescence. In the case of hexamethyl viologen, it is possible these additional methyls are protecting groups that prevent the hydroxide addition. Work is underway to extend these simulations (both to longer times and also to related species) in order to develop a complete model for this type of reactivity. Finally, it is important to remember that the simulations reported here are adiabatic on the S_1 state and do not include the entire photochemical process. While the most important steps with respect to the acid/base reaction that occurs between photoexcited MV^{2+} and water are included, the cascade from the optically accessible S_3 state to the photoacidic S_1 state as well as the final decay to S_0 are not studied. The nonadiabatic dynamics simulations, which would be needed to study the photochemistry of MV^{2+} from photoexcitation to decay back to the ground state, are also being pursued.

ASSOCIATED CONTENT

Supporting Information

The Supporting Information is available free of charge on the ACS Publications website at DOI: 10.1021/jacs.5b08177.

Assessment of the accuracy of FOMO-CASCI for the excited states of MV^{2+}, a test of Kasha's rule for the cascade from S_3 to S_1, additional results from the excited-state molecular dynamics simulations, and some optimized geometries of methyl viologen (PDF)

DOI: 10.1021/jacs.5b08177
J. Am. Chem. Soc. 2016, 138, 1868−1876

AUTHOR INFORMATION

Corresponding Author

*ehohenstein@ccny.cuny.edu

Notes

The authors declare no competing financial interest.

ACKNOWLEDGMENTS

This work was supported by startup funding provided by the Martin & Michele Cohen Fund for Science. E.G.H. would also like to thank Prof. Todd Martínez and Prof. Bern Kohler for helpful discussions and a critical reading of the manuscript.

REFERENCES

(1) Förster, T. *Z. Electrochem., Angew. Phys. Chem.* **1950**, *54*, 42−46.
(2) Förster, T. *Z. Electrochem., Angew. Phys. Chem.* **1950**, *54*, 531−535.
(3) Weller, A. *Z. Elektrochem.* **1952**, *56*, 662−668.
(4) Weller, A. *Z. Elektrochem.* **1954**, *58*, 849−853.
(5) Pines, E.; Huppert, D. *Chem. Phys. Lett.* **1986**, *126*, 88−91.
(6) Pines, E.; Huppert, D. *J. Chem. Phys.* **1986**, *84*, 3576−3577.
(7) Pines, E.; Huppert, D.; Agmon, N. *J. Chem. Phys.* **1988**, *88*, 5620−5630.
(8) Agmon, N.; Huppert, D.; Masad, A.; Pines, E. *J. Phys. Chem.* **1991**, *95*, 10407−10413.
(9) Tran-Thi, T.-H.; Gustavsson, T.; Prayer, C.; Pommeret, S.; Hynes, J. T. *Chem. Phys. Lett.* **2000**, *329*, 421−430.
(10) Rini, M.; Magnes, B.-Z.; Pines, E.; Nibbering, E. T. J. *Science* **2003**, *301*, 349−352.
(11) Mohammed, O. F.; Pines, D.; Dreyer, J.; Pines, E.; Nibbering, E. T. J. *Science* **2005**, *310*, 83−86.
(12) Leiderman, P.; Genosar, L.; Huppert, D. *J. Phys. Chem. A* **2005**, *109*, 5965−5977.
(13) Spry, D. B.; Fayer, M. D. *J. Chem. Phys.* **2008**, *128*, 084508.
(14) Tolbert, L. M.; Solntsev, K. M. *Acc. Chem. Res.* **2002**, *35*, 19−27.
(15) Webb, S. P.; Philips, L. A.; Yeh, S. W.; Tolbert, L. M.; Clark, J. H. *J. Phys. Chem.* **1986**, *90*, 5154−5164.
(16) Tolbert, L. M.; Haubrich, J. E. *J. Am. Chem. Soc.* **1990**, *112*, 8163−8165.
(17) Droz, R.; Knochenmuss, R.; Leutwyler, S. *J. Chem. Phys.* **1990**, *93*, 4520−4532.
(18) Tolbert, L. M.; Haubrich, J. E. *J. Am. Chem. Soc.* **1994**, *116*, 10593−10600.
(19) Knochenmuss, R.; Smith, D. R. *J. Chem. Phys.* **1994**, *101*, 7327−7336.
(20) Carmeli, I.; Huppert, D.; Tolbert, L. M.; Haubrich, J. E. *Chem. Phys. Lett.* **1996**, *260*, 109−114.
(21) Huppert, D.; Tolbert, L. M.; Linares-Samaniego, S. *J. Phys. Chem. A* **1997**, *101*, 4602−4605.
(22) Pines, E.; Pines, D.; Barak, T.; Magnes, B.-Z.; Tolbert, L. M.; Haubrich, J. E. *Ber. Bunsen-Ges. Phys. Chem.* **1998**, *102*, 511−517.
(23) Solntsev, K. M.; Huppert, D.; Tolbert, L. M.; Agmon, N. *J. Am. Chem. Soc.* **1998**, *120*, 7981−7982.
(24) Solntsev, K. M.; Huppert, D.; Agmon, N. *J. Phys. Chem. A* **1999**, *103*, 6984−6997.
(25) Knochenmuss, R.; Fischer, I.; Lührs, D.; Lin, Q. *Isr. J. Chem.* **1999**, *39*, 221−230.
(26) Solntsev, K. M.; Huppert, D.; Agmon, N.; Tolbert, L. M. *J. Phys. Chem. A* **2000**, *104*, 4658−4669.
(27) Knochenmuss, R.; Solntsev, K. M.; Tolbert, L. M. *J. Phys. Chem. A* **2001**, *105*, 6393−6401.
(28) Kim, T. G.; Topp, M. R. *J. Phys. Chem. A* **2004**, *108*, 10060−10065.
(29) Solntsev, K. M.; Clower, C. E.; Tolbert, L. M.; Huppert, D. *J. Am. Chem. Soc.* **2005**, *127*, 8534−8544.
(30) Pérez-Lustres, J. L.; Kovalenko, S. A.; Mosquera, M.; Senyushkina, T.; Flasche, W.; Ernsting, N. P. *Angew. Chem., Int. Ed.* **2005**, *44*, 5635−5639.
(31) Pérez-Lustres, J. L.; Rodriguez-Prieto, F.; Mosquera, M.; Senyushkina, T.; Ernsting, N. P.; Kovalenko, S. A. *J. Am. Chem. Soc.* **2007**, *129*, 5408−5418.
(32) Bhattacharya, B.; Samanta, A. *J. Phys. Chem. B* **2008**, *112*, 10101−10106.
(33) Presiado, I.; Karton-Lifshin, N.; Erez, Y.; Gepshtein, R.; Shabat, D.; Huppert, D. *J. Phys. Chem. A* **2012**, *116*, 7353−7363.
(34) Simkovitch, R.; Karton-Lifshin, N.; Shomer, S.; Shabat, D.; Huppert, D. *J. Phys. Chem. A* **2013**, *117*, 3405−3413.
(35) Simkovitch, R.; Shomer, S.; Gepshtein, R.; Shabat, D.; Huppert, D. *J. Phys. Chem. A* **2014**, *118*, 1832−1840.
(36) Simkovitch, R.; Shomer, S.; Gepshtein, R.; Huppert, D. *J. Phys. Chem. B* **2015**, *119*, 2253−2262.
(37) Arnaut, L. G.; Formosinho, S. J. *J. Photochem. Photobiol., A* **1993**, *75*, 1−20.
(38) Formosinho, S. J.; Arnaut, L. G. *J. Photochem. Photobiol., A* **1993**, *75*, 21−48.
(39) Hynes, J. T.; Tran-Thi, T.-H.; Granucci, G. *J. Photochem. Photobiol., A* **2002**, *154*, 3−11.
(40) Agmon, N. *J. Mol. Liq.* **2000**, *85*, 87−96.
(41) Agmon, N. *J. Phys. Chem. A* **2005**, *109*, 13−35.
(42) Abbruzzetti, S.; Viappiani, C.; Small, J. R.; Libertini, L. J.; Small, E. W. *Biophys. J.* **2000**, *79*, 2714−2721.
(43) Shum, P.; Kim, J.-M.; Thompson, D. H. *Adv. Drug Delivery Rev.* **2001**, *53*, 273−284.
(44) Nunes, R. M. D.; Pineiro, M.; Arnaut, L. G. *J. Am. Chem. Soc.* **2009**, *131*, 9456−9462.
(45) Emond, M.; Le Saux, T.; Maurin, S.; Baudin, J.-B.; Plasson, R.; Jullien, L. *Chem. - Eur. J.* **2010**, *16*, 8822−8831.
(46) Abeyrathna, N.; Liao, Y. *J. Am. Chem. Soc.* **2015**, *137*, 11282−11284.
(47) Chattoraj, M.; King, B. A.; Bublitz, G. U.; Boxer, S. G. *Proc. Natl. Acad. Sci. U. S. A.* **1996**, *93*, 8362−8367.
(48) Stoner-Ma, D.; Jaye, A. A.; Matousek, P.; Towrie, M.; Meech, S. R.; Tonge, P. J. *J. Am. Chem. Soc.* **2005**, *127*, 2864−2865.
(49) Stoner-Ma, D.; Melief, E. H.; Nappa, J.; Ronayne, K. L.; Tonge, P. J.; Meech, S. R. *J. Phys. Chem. B* **2006**, *110*, 22009−22018.
(50) Yu, H.-T.; Colucci, W. J.; McLaughlin, M. L.; Barkley, M. D. *J. Am. Chem. Soc.* **1992**, *114*, 8449−8454.
(51) Chen, Y.; Barkley, M. D. *Biochemistry* **1998**, *37*, 9976−9982.
(52) Henrich, J. D.; Suchyta, S.; Kohler, B. *J. Phys. Chem. B* **2015**, *119*, 2737−2748.
(53) Dodge, A. D. *Endeavour* **1971**, *30*, 130−135.
(54) Moradpour, A.; Amouyal, E.; Keller, P.; Kagan, H. *Nouv. J. Chim.* **1978**, *2*, 547−549.
(55) Crutchley, R. J.; Lever, A. B. P. *J. Am. Chem. Soc.* **1980**, *102*, 7128−7129.
(56) Gurunathan, K.; Maruthamuthu, P. *Int. J. Hydrogen Energy* **1995**, *20*, 287−295.
(57) Bard, A. J.; Fox, M. A. *Acc. Chem. Res.* **1995**, *28*, 141−145.
(58) Jana, A. K. *J. Photochem. Photobiol., A* **2000**, *132*, 1−17.
(59) Nada, A. A.; Hamed, H. A.; Barakat, M. H.; Mohamed, N. R.; Veziroglu, T. N. *Int. J. Hydrogen Energy* **2008**, *33*, 3264−3269.
(60) Watanabe, T.; Honda, K. *J. Phys. Chem.* **1982**, *86*, 2617−2619.
(61) Peon, J.; Tan, X.; Hoerner, J. D.; Xia, C.; Luk, Y. F.; Kohler, B. *J. Phys. Chem. A* **2001**, *105*, 5768−5777.
(62) Novakovic, V.; Hoffman, M. Z. *J. Am. Chem. Soc.* **1987**, *109*, 2341−2346.
(63) Rieger, A. L.; Edwards, J. O. *J. Org. Chem.* **1988**, *53*, 1481−1485.
(64) Garavelli, M.; Bernardi, F.; Olivucci, M.; Vreven, T.; Klein, S.; Celani, P.; Robb, M. A. *Faraday Discuss.* **1998**, *110*, 51−70.
(65) Worth, G. A.; Robb, M. A. *Adv. Chem. Phys.* **2002**, *124*, 355−431.
(66) Virshup, A. M.; Punwong, C.; Pogorelov, T. V.; Lindquist, B. A.; Ko, C.; Martinez, T. J. *J. Phys. Chem. B* **2009**, *113*, 3280−3291.
(67) Plasser, F.; Barbatti, M.; Aquino, A. J. A.; Lischka, H. *Theor. Chem. Acc.* **2012**, *131*, 1073.
(68) Geissler, P. L.; Dellago, C.; Chandler, D.; Hutter, J.; Parrinello, M. *Science* **2001**, *291*, 2121−2124.

DOI: 10.1021/jacs.5b08177
J. Am. Chem. Soc. 2016, 138, 1868−1876

(69) Park, J. M.; Laio, A.; Iannuzzi, A.; Parrinello, M. *J. Am. Chem. Soc.* **2006**, *128*, 11318−11319.
(70) Thomas, V.; Rivard, U.; Maurer, P.; Bruhács, A.; Siwick, B. J.; Iftimie, R. *J. Phys. Chem. Lett.* **2012**, *3*, 2633−2637.
(71) Bekçioğlu, G.; Hoffmann, F.; Sebastiani, D. *J. Phys. Chem. A* **2015**, *119*, 9244−9251.
(72) Isborn, C. M.; Luehr, N.; Ufimtsev, I. S.; Martínez, T. J. *J. Chem. Theory Comput.* **2011**, *7*, 1814−1823.
(73) Hohenstein, E. G.; Luehr, N.; Ufimtsev, I. S.; Martínez, T. J. *J. Chem. Phys.* **2015**, *142*, 224103.
(74) Ufimtsev, I. S.; Martínez, T. J. *J. Chem. Theory Comput.* **2008**, *4*, 222−231.
(75) Ufimtsev, I. S.; Martínez, T. J. *J. Chem. Theory Comput.* **2009**, *5*, 1004−1015.
(76) Ufimtsev, I. S.; Martínez, T. J. *J. Chem. Theory Comput.* **2009**, *5*, 2619−2628.
(77) Granucci, G.; Toniolo, A. *Chem. Phys. Lett.* **2000**, *325*, 79−85.
(78) Granucci, G.; Persico, M.; Toniolo, A. *J. Chem. Phys.* **2001**, *114*, 10608.
(79) Toniolo, A.; Ben-Nun, M.; Martínez, T. J. *J. Phys. Chem. A* **2002**, *106*, 4679−4689.
(80) Slavíček, P.; Martínez, T. J. *J. Chem. Phys.* **2010**, *132*, 234102.
(81) Gidopoulos, N.; Theophilou, A. *Philos. Mag. B* **1993**, *69*, 1067−1074.
(82) Gidopoulos, N. I.; Papaconstantinou, P. G.; Gross, E. K. U. *Phys. B* **2002**, *318*, 328−332.
(83) Roos, B. O. *Adv. Chem. Phys.* **1987**, *69*, 399−445.
(84) Finley, J.; Malmqvist, P.-A.; Roos, B. O.; Serrano-Andrés, L. *Chem. Phys. Lett.* **1998**, *288*, 299−306.
(85) Roos, B. O. *Acc. Chem. Res.* **1999**, *32*, 137−144.
(86) Warshel, A.; Levitt, M. *J. Mol. Biol.* **1976**, *103*, 227−249.
(87) Jorgensen, W. L.; Chandrasekhar, J.; Madura, J. D.; Impey, R. W.; Klein, M. L. *J. Chem. Phys.* **1983**, *79*, 926−935.
(88) Grimme, S.; Antony, J.; Ehrlich, S.; Krieg, H. *J. Chem. Phys.* **2010**, *132*, 154104.
(89) Kasha, M. *Discuss. Faraday Soc.* **1950**, *9*, 14−19.
(90) The computations used one 6-core Intel Core i7-4930K processor clocked at 3.4 GHz, 32 GB of memory, and four NVIDIA GeForce GTX 970 GPUs.
(91) Tully, J. C. *J. Chem. Phys.* **1990**, *93*, 1061.
(92) Martínez, T. J.; Ben-Nun, M.; Levine, R. D. *J. Phys. Chem.* **1996**, *100*, 7884−7895.
(93) Ben-Nun, M.; Quenneville, J.; Martínez, T. J. *J. Phys. Chem. A* **2000**, *104*, 5161.
(94) Mau, A. W.-H.; Overbeek, J. M.; Loder, J. W.; Sasse, W. H. F. *J. Chem. Soc., Faraday Trans. 2* **1986**, *82*, 869−876.
(95) Hopkins, A. S.; Ledwith, A.; Stam, M. F. *J. Chem. Soc. D* **1970**, *82*, 494−495.

DOI: 10.1021/jacs.5b08177
J. Am. Chem. Soc. 2016, 138, 1868−1876